CHAPTER 9

Characterising RNA Dynamics using NMR Residual Dipolar Couplings

CATHERINE D. EICHHORN, SHAN YANG AND HASHIM M. AL-HASHIMI*

Department of Chemistry & Biophysics, The University of Michigan, Ann Arbor, MI 48109, USA
*E-mail: hashimi@umich.edu

9.1 Introduction

Our basic understanding of RNA's role in biology has changed profoundly over the past decade with the discovery of non-coding RNA molecules (ncRNAs) as abundant players in gene expression and regulation.[1–4] Accompanying these discoveries has been the growing realisation that most regulatory RNA molecules do not fold into a single native conformation, but rather, can adopt many different conformations along a free-energy landscape.[5–8] These distinct conformations are often preferentially stabilised by cellular cues to effect a given biological function.[6,7,9] For example, riboswitches are a new class of regulatory RNA molecules, typically located in the 5′ untranslated region of genes, that transition between different secondary structures to regulate the expression of genes in response to a wide range of cellular stimuli.[10,11] Beyond understanding function, RNA is increasing in its importance as a drug target[12] and a dynamic view of RNA structure is essential for successfully applying structure-based approaches in

RSC Biomolecular Sciences No. 25
Recent Developments in Biomolecular NMR
Edited by Marius Clore and Jennifer Potts

Published by the Royal Society of Chemistry, www.rsc.org

lead compound discovery and optimisation.[7,13–15] Experimental data that probes deeply into dynamic aspects of RNA structure at atomic resolution over extended timescales is also required to guide developments in computational force fields, which remain severely underdeveloped for nucleic acids.[16,17]

Among several NMR techniques that have been developed and applied to study RNA dynamics,[6,8,18,19] the measurement of residual dipolar couplings (RDCs) in partially aligned systems[20–23] is providing new insights into previously poorly understood aspects of RNA dynamics behavior. There are several factors that make RDCs attractive probes of RNA dynamics. First, RDCs can be measured in great abundance between nuclei in base, sugar and backbone moieties without some of the complications that plague measurements of NMR spin relaxation and relaxation dispersion data. Second, the timescale sensitivity of RDCs to internal motions extends from picoseconds to milliseconds and uniquely allows insights into dynamics occurring at nanosecond to microsecond timescales that are difficult to access by NMR spin-relaxation methods. Finally, by changing the alignment properties of a target RNA molecule, more than one RDC data set can be measured,[24,25] providing the basis for mapping out complex 3D motional choreographies with high spatial resolution.[26–29] Although RDCs continue to be used primarily as a rich source of long-range orientational constraints for improving the quality of structures determined by solution-state NMR,[30–33] a growing number of studies are exploiting the unique dynamics sensitivity of RDCs,[6,18,23] Here, we review NMR RDC methods for studying RNA dynamics and highlight some of the new insights that have been obtained.

9.2 Residual Dipolar Coupling Theory

The theoretical underpinnings of dipolar and other anisotropic interactions have been reviewed extensively both in the context of early liquid–crystal applications[34–44] and biomolecular applications.[32,45–50] Here we briefly review the basic theory underpinning RDCs with a specific emphasis on nucleic acid dynamics applications.

9.2.1 The Dipolar Interaction

Analogous to a pair of bar magnets, nuclear dipole–dipole interactions originate from the through-space magnetic interaction between two nuclei, where the local magnetic field at a given nucleus is perturbed by the magnetic field of a neighboring nucleus. Consider how the dipolar interaction between a carbon and proton nucleus in a C–H bond modulates the effective magnetic field at the carbon nucleus [Figure 9.1(A)]. The carbon nucleus experiences the sum of the static external magnetic field and the much smaller ($\sim 10^{-4}$) magnetic field generated by the proton nucleus. Because the nuclear bar magnets are always quantised parallel (or anti-parallel) to the magnetic field, the proton-induced magnetic field experienced by the carbon nucleus will vary

as the C–H bond changes orientation relative to the magnetic field, either due to internal or overall motions; in some orientations the proton field adds to the external magnetic field, whereas in other orientations it subtracts or has no contribution [Figure 9.1(A)]. This angular dependence is described by $\langle\frac{3\cos^2\theta-1}{2}\rangle$, where θ is the angle between the inter-nuclear vector and the magnetic field, and the angular brackets denote a time-average over all orientations sampled at a rate faster than the dipolar coupling [Figure 9.1(B)].

Under conditions of random molecular tumbling, the angular term averages to zero and the proton does not affect the average field at the carbon nucleus; therefore, the observed carbon frequency is unchanged. As a result, RDCs are not observable under normal solution conditions. However, by imparting a small degree of order on the molecule, the angular term no longer averages to zero, and the carbon nucleus experiences a residual proton field in addition to the external magnetic field. Since half of the proton nuclei are aligned parallel and the other half anti-parallel to the field, the proton fields add to the external

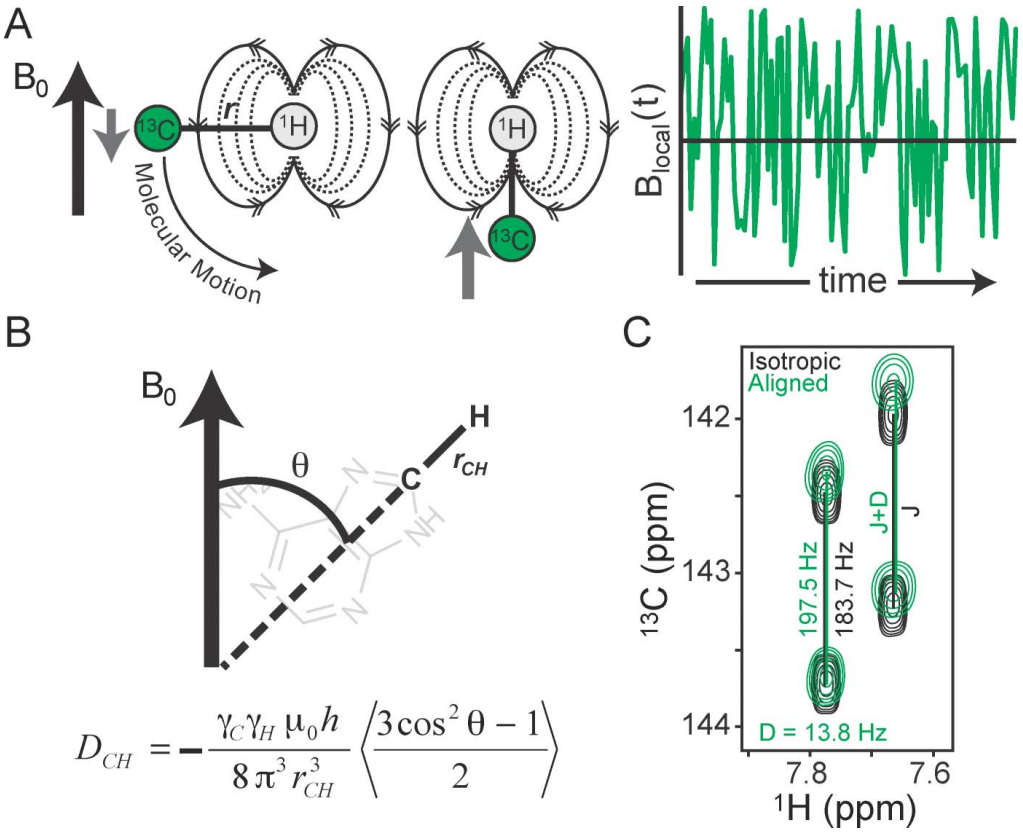

$$D_{CH} = -\frac{\gamma_C \gamma_H \mu_0 h}{8\pi^3 r_{CH}^3}\left\langle\frac{3\cos^2\theta - 1}{2}\right\rangle$$

Figure 9.1 Physical origin and measurement of RDCs. (A) The reorientation of bond vectors leads to an oscillating local magnetic field at the nucleus of interest. (B) RDCs between spins *i* and *j* (C and H, respectively) provide long-range constraints on the average orientation (θ) of the internuclear bond vector relative to the magnetic field (B_0). (C) Measurement of RDCs as new contributions to resonance splittings (black resonances) observed upon partial alignment (green resonances).

field for half of the carbon nuclei and subtract for the other half.[51] Consequently, the carbon resonance frequency splits into a doublet, reflecting the addition and subtraction of the average proton field. The magnitude of this splitting is referred to as a 'residual dipolar coupling'.[20,52] Through-space dipolar couplings (D) and through-bond scalar couplings (J) both effectively increase or decrease the average magnetic field at a given nucleus, which manifests in a splitting of resonances. This makes it possible to readily measure RDCs as new contributions to splittings when a molecule is partially aligned [Figure 9.1(C)].

At high magnetic fields, the dipolar interaction can be simplified to a truncated dipolar Hamiltonian,[53,54] resulting in the following expression (in Hz) describing the local field contribution between nuclei i and j:

$$D_{ij} = -\left(\frac{\mu_0}{4\pi}\right)\frac{\gamma_i\gamma_j h}{2\pi^2 r_{ij,\mathrm{eff}}^3}\left\langle\frac{3\cos^2\theta - 1}{2}\right\rangle, \quad (1)$$

where μ_0 is the magnetic permittivity of a vacuum, h is Planck's constant, r_{ij} is the inter-nuclear distance between the spins, and γ is the gyromagnetic ratio. The angular bracket denotes a time average over all orientations sampled, while distance averaging of the inter-nuclear distance is represented by the effective bond length $r_{ij,\mathrm{eff}}$.[55–57]

The utility of RDCs in studies of dynamics arises chiefly from the angular dependence of eqn (1),[22] rendering RDCs sensitive to internal motions that re-orient bond vectors at timescales faster than the inverse of the dipolar interaction. For typical levels of alignment, this encompasses a wide range of timescales spanning picoseconds to $\sim$10 milliseconds.[22] Although RDCs do not provide information about motional timescales, they are exquisitely sensitive to the orientation distribution sampled by the bond vector and, therefore, the 3D choreography of the motion.[23,50,58] In addition, a wide variety of RDCs can be measured in nucleic acids (C–H, C–C, C–N, N–H, H–H, P–H, *etc.*), providing the basis for comprehensively mapping out nucleobase, sugar, and phosphodiester backbone dynamics.

9.2.2 The Alignment Tensor

Central to the dynamic interpretation of RDCs is a description of the overall alignment of a molecule and specifically, the contributions to the angular term, $\left\langle\frac{3\cos^2\theta - 1}{2}\right\rangle$, arising due to overall re-orientation. In general, overall re-orientation dominates the averaging of this angular term, scaling its value down by a factor 10^{-4} compared to typically only 10^{-1} due to internal motions. The overall alignment of an internally rigid molecule relative to the magnetic field and any observed RDCs can be fully accounted for by specifying five elements of a traceless and symmetric overall order or alignment tensor.[21,41] The order tensor describes the orientation distribution of the axially symmetric magnetic field direction relative to the chiral molecular

frame. The physical significance of the order tensor can be best understood using a Cartesian representation, S_{kl}.[41] Two angular terms define the orientation of a principal direction of order, S_{zz}, relative to the chiral molecular fragment. The S_{zz} axis defines the average orientation of the magnetic field relative to the fragment; it is oriented on average along and perpendicular to the magnetic field direction for $S_{zz} > 0$ and $S_{zz} < 0$, respectively. A third angular term specifies the orientation of S_{xx}/S_{yy} axes with S_{yy} pointing along the direction of asymmetry (*i.e.*, the direction about which the magnetic field is most likely to rotate about compared to other axes perpendicular to S_{zz}). An order parameter, referred to as the generalised degree of order (ϑ)[59] describes the degree of alignment ($\vartheta = \sqrt{\frac{2}{3}\left(S_{xx}^2 + S_{yy}^2 + S_{zz}^2\right)}$) and the extent to which the magnetic field direction is ordered relative to the molecule. Finally, an asymmetry parameter ($\eta = \frac{S_{xx} - S_{yy}}{S_{zz}}$) describes the extent of asymmetry in the distribution of the magnetic field direction relative to the chiral frame [Figure 9.2(A)]. When in the principal axis system (PAS) of the order tensor, the two order parameters are frequently expressed in terms of a magnitude, D_a and rhombicity, R [21]:

$$D_a^{ij} = -\left(\frac{\mu_0}{4\pi}\right)\frac{\gamma_i\gamma_j h}{2\pi^2 r_{ij}^3}\left(\frac{1}{2}S_{zz}\right); \qquad R = \frac{2}{3}\eta \tag{2}$$

A similar order/alignment tensor type description can be used to describe internal motions within the molecule; however, in this case one describes the average orientation of an axially symmetric RDC bond vector or an axially asymmetric fragment relative to the chiral molecular frame. The dynamics interpretation of RDCs is discussed in greater detail in Section 9.5.

For a rigid object, the time-averaged angular term in eqn (1) can be expressed in terms of a time-independent orientation of the internuclear vector relative to an arbitrary frame and the five-order tensor elements (S_{kl}):[41,60]

$$\left\langle \frac{3\cos^2\theta - 1}{2} \right\rangle = \sum_{kl=xyz} S_{kl}\cos(\alpha_k)\cos(\alpha_l), \tag{3}$$

where α_n is the angle between the ij^{th} internuclear vector and the n^{th} axis of arbitrarily defined coordinates. In practice, the overall order/alignment tensor can be determined for a solute molecule provided the measurement of five or more spatially independent RDCs for bond vectors that do not undergo internal motions and whose relative orientation (but not necessarily translation) within the structure is known.

9.3 Partial Alignment of Nucleic Acids

The measurement of RDCs under solution conditions hinges on being able to introduce a particular level of alignment,[61] either by dissolving the solute in an

ordering medium[21] or in the case of nucleic acids and paramagnetic proteins, through direct interactions with the magnetic field itself.[20,44] Alignment levels $\leq 10^{-5}$ (*i.e.*, corresponding to 1 in 10^5 molecules being completely aligned) lead to RDCs that are too small compared to NMR linewidths to allow precise measurements. Much higher degrees of alignment ($\geq 10^{-2}$) give rise to extensive dipolar couplings, compromising the spectral resolution required to analyse large biomolecules. In general, alignment levels on the order of $\sim 10^{-3}$ are optimal.[21,61] At this degree of alignment, a wide range of RDCs can be measured with a favorable magnitude-to-precision ratio while maintaining spectral resolution. A smaller subset of RDCs can be measured with alignment levels $\sim 10^{-4}$ with less than optimum magnitude-to-precision ratios.

9.3.1 Ordering Media-Induced Alignment

It is now relatively straightforward to achieve alignment levels $\sim 10^{-3}$ in solution NMR by dissolving the biomolecule of interest in an inert ordering media[21,51,62] [Figure 9.2(A)]. This was first demonstrated using liquid crystalline disc-shaped phospholipids called 'bicelles'[21] which were previously used as a mimic of membrane bilayers in studies of membrane-associated biomolecules.[63,64] While this neutral bicelle medium has been used in nucleic acid studies, other media have since been introduced which have become more popular. We provide a summary of ordering media used to date for aligning nucleic acids in Table 9.1.

Since nucleic acids are highly negatively charged, the charge properties of the ordering medium are an important consideration. For example, positively charged ordering media may lead to undesirable interactions with nucleic acid solutes. For nucleic acid applications, the ordering medium must also be tolerant to high ionic strength conditions. The most commonly used ordering medium that satisfies the above requirements is the commercially available filamentous Pf1 bacteriophage, which induces alignment through electrostatic and steric mechanisms [Figure 9.2(A)].[65–67]

Pf1 phage is composed of a 7.4 kb circular, single-stranded DNA genome and has a rod-like shape, estimated to be $\sim$20 000 Å long and $\sim$60 Å in diameter.[67] Pf1 phage is highly robust, having favorable properties largely due to its lower nematic threshold.[68,69] Its coat proteins are negatively charged, reducing the potential for adverse interactions with nucleic acids. Since polyanionic nucleic acids have a semi-uniform charge distribution,[68,70] the steric and electrostatic contributions from phage are thought to have similar roles,[68,70] generally aligning nucleic acids with the principal direction of order (S_{zz}) oriented along the long axis of the molecule. Positive alignment ($S_{zz} > 0$) is expected for elongated nucleic acids with S_{zz} being, on average, oriented along the magnetic field direction [Figure 9.2(A)]. Experimentally, RDCs are calculated from the difference in splittings measured in the absence (J) and presence ($J + D$) of Pf1 phage [Figure 9.1(C)]. The optimum phage concentration is typically $\sim$20 mg mL^{-1} but can vary depending on the

Table 9.1 Alignment media used in studies of nucleic acids.

Ordering medium	*Temperature range/°C*	*Notes*
DMPC:DHPC ('bicelles')[21,161]	27–45	Perpendicular alignment disk-like shape. Neutral, sensitive to ionic conditions. The charge can be modified to be positive or negative with addition of CTAB or SDS respectively. More stable ether-based bicelles can also be prepared.
Rod-shaped viruses (Pf1 phage and TMV)[65–67]	5–60	Parallel alignment rod-like shape. Negatively charged, stable in pH >5, and aggregates at high salt concentration. Sample is recoverable. Most widely used.
Purple membrane[162,163]	−269–69	Parallel alignment disk-like shape. Stable in pH range 2.5 to 10, and salt concentrations up to 5 M. Sample is recoverable.
Polyacrylamide gels[164,165]	5–45	Mechanical gel. Very stable and inert. The charge can be modified to be positive or negative with addition of DADMAC or acrylate respectively. Sample is recoverable.
n-Alkyl-poly(ethylene glycol)/ *n*-alkyl alcohol or glucopone/ *n*-hexanol (PEG)[166,167]	0–40	Perpendicular alignment lamellar shape. Insensitive to pH, and moderately sensitive to salt concentrations.

shape of the target nucleic acid. Generally, domain elongated RNA molecules[71] require lower phage concentrations (5–10 mg mL^{-1}) to achieve the optimum level of alignment, whereas smaller potentially more isotropic RNA molecules, such as single strands, can require concentrations as high as 50 mg mL^{-1}.[72] The phage concentration in the NMR sample can be estimated by dividing the observed deuterium residual quadrupolar splitting by a factor of 0.886 or by measuring the UV–vis absorbance at 270 nm using an extinction coefficient of 2.25 cm·mL mg^{-1}.[67]

For proteins, the overall alignment can be modulated by changing the shape and electrostatic properties of the ordering medium used[24,25] or, by applying site-specific mutations that alter the electrostatic properties of the solute protein without affecting its functional structure.[24] This allows the measurement of multiple independent sets of RDCs from which much more information can be obtained regarding the dynamics of bond vectors[24–26,28,73] (see Section 9.5). Attempts at using different ordering media to induce independent alignments of nucleic acids have so far been unsuccessful,[74,75] likely because the uniform negative charge distribution follows that of the overall molecular shape more

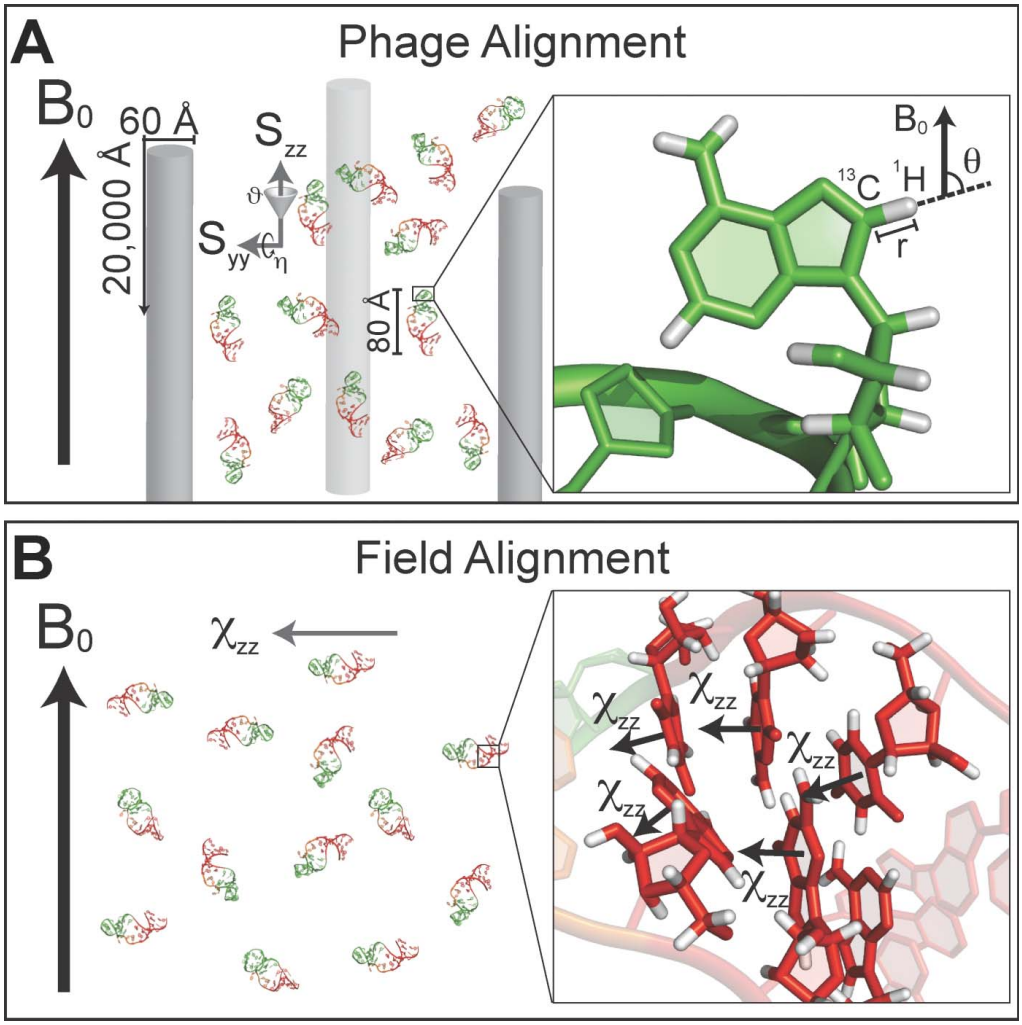

Figure 9.2 Approaches to induce partial molecular alignment using (A) ordering media such as Pf1 phage (shown in grey), which transmits order through a combination of steric and electrostatic mechanisms, and (B) magnetic field alignment due to the constructive addition of anisotropic magnetic susceptibility tensors (χ) in the nucleobases.

closely, making it difficult to independently alter shape and electrostatic contributions to alignment.

The development of methods to modulate nucleic acid alignment is of key importance in enabling the extraction of the full dynamics information contained within RDCs and also in increasing the data density to allow robust cross-validation of any generated dynamic models. We can identify two avenues to achieve independent alignment of nucleic acids. First, magnetic field alignment, discussed below, has been shown to yield distinct alignments as compared to ordering media.[76,77] Second, the systematic elongation of RNA terminal helices, which affords a change in the shape of the solute, has also been shown to modulate the overall alignment of an RNA molecule.[78]

9.3.2 Magnetic-Field-Induced Alignment

Another method for aligning nucleic acids involves spontaneous alignment from interactions with the magnetic field itself.[35,52] Some of the first studies measuring anisotropic interactions of biomolecules relied on the spontaneous field alignment of molecules with large magnetic susceptibility anisotropies ($\Delta\chi$), with nucleic acids as well as paramagnetic proteins being primary targets.[20,35,52,79,80] In nucleic acids, the diamagnetic susceptibility primarily originates from the aromatic nucleobases, in which the circulation of π-orbital electrons in response to the magnetic field creates an induced dipole moment, which then re-interacts with the magnetic field, causing an anisotropic preference in the molecular orientation [Figure 9.2(B)]. The degree of alignment depends on $\Delta\chi$ as well as the square of magnetic field strength (B_0^2).

While the magnetic susceptibilities of individual bases are not adequate to induce a useful degree of alignment (*ca.* 2–7 $\times$ 10^{-6} at 800 MHz field strength), their constructive addition, particularly in helices in which bases are nearly co-axially stacked, enhances the total anisotropy and resulting degree of order (typically 10^{-4} at 800 MHz). Importantly, the net principal χ-tensor direction (χ_{zz}) need not be coincident with the long axis of the molecule, and therefore the S_{zz} direction, providing a useful approach for measuring a second independent RDC data set.[75,77,81] Unlike the phage-ordering medium, which typically orients RNA such that the long axis is on average oriented along the magnetic field, the diamagnetic alignment of nucleic acids is generally negative ($\chi_{zz} < 0$) with the χ_{zz} direction being, on average, oriented perpendicular to the magnetic field [Figure 9.2(B)] although under certain conditions it is possible to have conformations with positive alignment ($\chi_{zz} > 0$).

For magnetic-field-induced alignment, the order tensor elements can be expressed in terms of the magnetic field strength (B_0), the χ-tensor (in units of m^3 per molecule), and temperature (T)[34,35,40,44]:

$$S_{zz} = \Delta\chi\left[\frac{B_0^2}{15\mu_0 kT}\right] \text{ and } S_{xx} - S_{yy} = \delta\chi\lfloor\frac{B_0^2}{10\mu_0 kT}\rfloor, \tag{4}$$

where

$$\Delta\chi = \chi_{zz} - \left(\frac{\chi_{xx} + \chi_{yy}}{2}\right) \text{ and } \delta\chi = \chi_{xx} - \chi_{yy}. \tag{5}$$

Field-induced RDCs are obtained by measuring splittings at several magnetic field strengths, preferably three or more. Splittings are plotted as a function of B_0^2 to back-calculate isotropic scalar couplings (J), *i.e.*, splittings at zero field. RDCs at a given field strength, typically the highest field, are then calculated by subtracting J from observed splittings ($J + D$). Apparent field RDCs can be measured from the difference in splittings at only two magnetic fields; however, eqn (5) must be adjusted accordingly.[82]

In practice, the requirement for measuring splittings at multiple fields decreases the number of RDCs that can be measured reliably given the decrease in spectral resolution at lower field strengths. Recently, Bax and co-workers showed that an approximate value for the scalar imino N–H scalar coupling (J_{NH}) in base-paired residues can be obtained based on the imino proton chemical shift, allowing the reliable measurement of field-induced RDCs at a single magnetic field strength.[77]

Another important consideration when measuring field-induced RDCs is that splittings have a field-dependent contribution from dynamic frequency shifts (DFS), which arise from the imaginary component of the spectral density function for cross-correlation between dipolar and chemical shift anisotropy relaxation mechanisms.[83,84] However, at fields $>$500 MHz, the DFS contribution to splittings is nearly constant (within 0.1 Hz), resulting in a relatively small contribution to the measured RDCs (typically $<$0.2 Hz for C–H and N–H RDCs measured at fields $\geq$500 MHz).

Even at current magnetic field strengths, the achievable degree of magnetic field alignment (10^{-4}) for typical RNA constructs (20–40 nt) is still an order of magnitude smaller than the optimal degree of alignment (10^{-3}). However, field alignment can allow measurement of an independent set of RDC data without having to use a potentially perturbing ordering medium.[81] The overall χ-tensor also has a relatively simple and well-known dependence on structure, and in particular, the orientation of nucleobases. This makes possible a number of unique applications such as the determination of nucleic acid stoichiometry,[81] derivation of the relative orientation of nucleic acid–protein complexes when the nucleic acid structure is known,[52,76] and determination of the absolute levels of internal dynamics.[85,86] Note that such applications often require accurate parameters for the nucleobase χ-tensors, and any uncertainty in these parameters need to be properly accounted for.[87] For larger and extended RNA molecules, more optimal levels of alignment may be achievable, particularly as the alignment grows quadratically with the ever-increasing magnetic field strength. For example, optimal alignment levels of 10^{-3} are in principle achievable at current field strength (900 MHz) for RNA on the order of 100 base pairs, and much larger RNA moleculess can now be studied by NMR spectroscopy.[23] We can therefore anticipate that field RDCs will continue to be important parameters in NMR studies of RNA structure and dynamics.

9.4 Measurement of RDCs in Nucleic Acids

Several experiments have been developed to measure a wide variety of RDCs in nucleic acids (see Table 9.2). The choice of RDCs to be measured is generally guided by the desire to maximise the magnitude-to-precision ratio and coverage of data throughout the RNA base, sugar and backbone moieties. The most commonly and easily measured RDCs are those between directly bonded C–H, N–H, and C–C nuclei in the nucleobases and also C1′–H1′ in the sugar moieties (Figure 9.3). For small RNA molecules, these directly bonded

Table 9.2 Pulse sequences for the measurement of RDCs in nucleic acids.

Pulse sequence	*Type of RDCs*	*Comments*
HC[C](C) hd-TROSY-E.COSY[96]	$^1D_{C2H2}$, $^1D_{C5H5}$, $^1D_{C6H6}$, $^1D_{C8H8}$, $^1D_{C4C5}$, $^1D_{C5C6}$, $^2D_{C5H6}$, $^2D_{C6H5}$ and $^2D_{C4H5}$	Pseudo-3D experiments for homonuclear decoupling employing TROSY and E.COSY elements.
CH_2-S^3E HSQC[108]	$^1D_{(C5\,H5'+C5'H5'')}$ and $^2D_{(H5'H5'')}$ (in DNA only $^1D_{(C2'H2'+C2'H2'')}$ and $^2D_{(H2'H2'')}$)	2D experiments with spin-state selection for detection of up- or downfield carbon components of CH_2 spin states.
3D S^3CT E.COSY[102]	$^1D_{C4'H4'}$, $^2D_{C5'H4'}$, $^1D_{(C5'H5'+C5'H5'')}$, ($^1D_{C5'H5'[']}$–$^2D_{H5'H5''}$), $^2D_{C4'H5'+C4'H5''}$, and $^3D_{H4'H5'[']}$	3D experiments for measuring RDCs in methine-methylene C–H pairs. One experiment yields eight splittings.
H1C1C2 E.COSY[101,168]	$^1D_{C1'H1'}$, $^1D_{C2'H2'}$, $^2D_{C1'H2'}$, $^2D_{C2'H1'}$, and $^3D_{H1'H2'}$	3D experiment utilising E.COSY for measuring five splittings in one experiment.
IPAP HN-HSQC, IPAP H(N)C-HSQC[88]	$^1D_{N1H1}$, $^1D_{N3H3}$, $^2D_{H1C2}$, $^2D_{H1C6}$, $^2D_{H3C2}$, and $^2D_{H3C4}$	2D experiments yielding 1–2 couplings per experiment.
3D IPAP-HCcH-COSY 3D relay-HCcH-COSY[104,168]	$^1D_{C2'H2'}$ and $^1D_{C3'H3'}$	Uses C1′H1′ to alleviate spectral overcrowding in the C2′H2′ and C3′H3′ region.
MQ-HCN[100]	$^1D_{C1'H1'}$, $^1D_{C1'N1/N9}$, $^1D_{C1'C2'}$, $^2D_{H1'N1/9}$, $^2D_{H1'C2'}$, $^2D_{H1'N1/9}$, $^1D_{C6H6}$, $^1D_{C6N1}$, $^1D_{C6C5}$, $^1D_{C8H8}$, $^1D_{C8N9}$, $^2D_{H8N9}$, $^2D_{H6N1}$, and $^2D_{H6C5}$	Suite of six MQ-based 3D experiments yielding 1–2 splittings per experiment.
S^3E IS[T][89]	^1D and ^2D	2D experiments for measuring most of the one- and two-bond splittings.
^{13}C–^1H TROSY[92]	$^1D_{C2H2}$, $^1D_{C5H5}$, $^1D_{C6H6}$, and $^1D_{C8H8}$	Sensitivity enhanced using TROSY and native ^{13}C magnetisation.
3D MQ/TROSY-HCN-QJ[103]	$^1D_{C1'N9}$, $^1D_{C8N9}$, $^1D_{C4N9}$, $^1D_{C1'N1}$, $^1D_{C6N1}$, and $^1D_{C2N1}$	3D quantitative *J*-modulated experiments for measuring one bond C–N splittings.
ARTSY[97]	$^1D_{N1H1}$, $^1D_{N3H3}$, $^1D_{C2H2}$, $^1D_{C5H5}$, $^1D_{C6H6}$, $^1D_{C8H8}$	Sensitivity enhanced TROSY-based 2D experiments for measuring one-bond N–H and C–H splittings

C–H and N–H splittings can be measured using 2D HSQC-type experiments that employ inphase–antiphase (IPAP) [88] or spin-selective excitation methods[89–91] to encode individual components of the doublet along the ^{13}C or ^{15}N dimension. For larger RNA molecules s (typically >40 nt), it can be advantageous to target the slowly relaxing TROSY ^{13}C or ^{15}N component

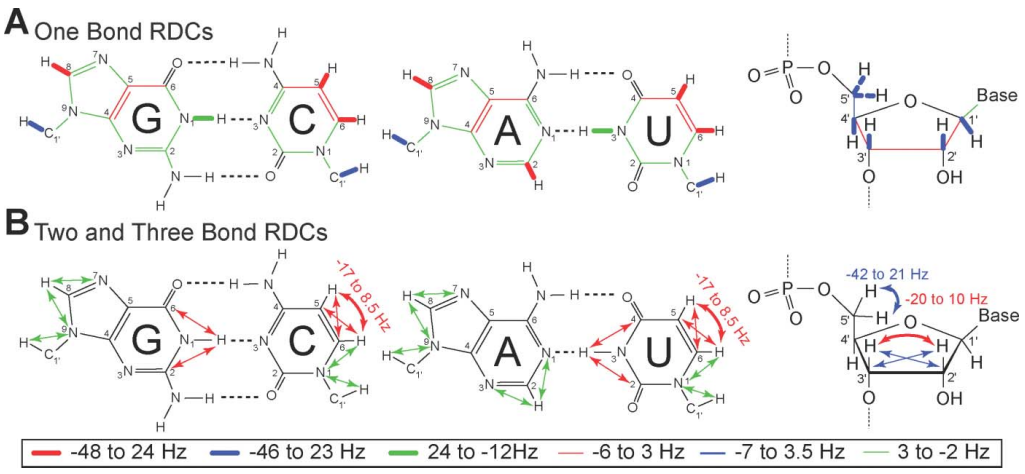

Figure 9.3 Commonly measured RDCs in nucleobase and sugar moieties using pulse sequences listed in Table 9.2. (A) One-bond C–H and N–H RDCs are most often measured due to their favorable magnitude, but smaller one-bond C–C and C–N as well as (B) two- and three-bond RDCs can be measured. Note that typically larger magnitude RDCs are shown as thick lines whereas smaller RDCs are shown as thin lines (see legend).

of the doublet for resonances in the nucleobase that have sizeable CSAs.[92–97] This can be achieved either by encoding individual components of the doublets along the ^{1}H dimension,[71,98,99] or through intensity-based measurements in TROSY-HSQC spectra with variable dephasing delays.[97] For example, by selecting the TROSY component, Bax and co-workers demonstrated the accurate measurement of C2H2, C5H5, C6H6, and C8H8 RDCs in the 60-nt MMLV dimer initiation site RNA.[99] Multi-dimensional experiments that employ HCN and E.COSY-type schemes can also be used to improve spectral resolution, particularly for sugar C1′ and nucleobase carbons and nitrogens.[96,100–103]

In general, measurement of C–H RDCs in sugar moieties (*e.g.*, C2′H2′, C3′H3′, C2′H3′, C3′H2′, C4′H4′, C5′H5′, C5′H5′′) is significantly more challenging because of severe spectral overlap in 2D C–H HSQC-type experiments. Experiments have been developed that exploit the better C1′H1′ resolution in measuring C2′H2′ and C3′H3′ RDCs.[104] Severe spectral overlap unfortunately also complicates the measurement of RDCs between ^{31}P and sugar protons[105,106] which can provide unique information on backbone conformation, a problem that is compounded by the deterioration of sensitivity at high magnetic fields due to sizeable ^{31}P CSA relaxation.

Pulse sequences have also been developed to allow the precise measurement of much smaller RDCs[96,103,107–109] For example, Bax and co-workers developed 3D HCN-type experiments for the measurement of very small (−2 to +3 Hz) C–N RDCs ($C_{1'}$–$N_{1/9}$, $C_{6/8}$–$N_{1/9}$, $C_{2/4}$–$N_{1/9}$) in a 24 nucleotide (nt) RNA and demonstrated the utility of these RDCs in determining small deviations from idealised A-form geometry.[103] Experiments that rely on the planarity and strong coupling between C6H6 and C5H5 bond vectors in

pyrimidine nucleobases have also been developed for the measurement of two-bond nucleobase C–H RDCs (C_5–H_6, C_6–H_5, C_4–H_5).[96] In general, the measurement of such small RDCs is only practical for small-to-moderate size RNA molecules (<30 nt) and can become challenging for much larger RNA molecules.

Experiments have also been developed to measure ^1H–^1H RDCs.[107–110] For example, Pardi and co-workers recently demonstrated the measurement of imino ^1H–^1H RDCs in a 29-nt IRE RNA, and showed their utility in differentiating geometric differences between GU and WC base pairs.[109] Bax and co-workers developed a CH_2-S^3E experiment to measure geminal H5′–H5′′ RDCs on a 24-nt RNA. By incorporating the 'Rance–Kay' transfer element,[111] undesired magnetisation transfers were suppressed more than 10-fold, leading to significantly narrowed ^1H linewidths and enabling the accurate measurement of RDCs between these methylene pairs.[108] The authors note that RDC values are negative in sign, similar to other sugar RDCs, and indicate that their orientation is parallel with respect to the helical axis, as expected for a helical geometry.[108] In another interesting application, experiments have been developed to detect and measure longer range ^1H–^1H RDCs between nuclei that are up to 12 Å apart.[107] These experiments use selective decoupling pulses to suppress line broadening contributions form ^1H–^1H dipolar couplings and thereby permit the accurate measurement of small (*ca.* 1 Hz) RDCs between the well-resolved sugar H1′ and nucleobase H5 nuclei.[107]

Selective labelling strategies have also been used to help overcome the spectral resolution problem in the measurement of RDCs. For example, Lukavsky and co-workers were able to nearly double the number of RDCs (compared to a uniformly $^{13}C/^{15}N$-labelled sample) for a 74-nt RNA by ligating a uniformly ^{15}N-labelled strand to an unlabelled strand.[112] In another interesting application, Luy and Marino incorporated ^{19}F into the sugar 2′-hydroxyl position of a 21-nt RNA at different sites and used these constructs to measure F–H ($F_{2'}$–$H_{2'}$, $F_{2'}$–$H_{1'}$, $F_{2'}$–$H_{3'}$, $F_{2'}$–H_6, $F_{2'}$–H_8) RDCs. The authors find that RDCs fit extremely well to an A-form geometry in helical regions, indicating that this probe does not perturb the helical geometry.[113]

Although not reviewed here, one can also measure a wide variety of residual chemical shift anisotropies (RCSAs) as a complement to RDCs.[99,114,115] Sizeable RCSAs can be measured in nucleobase carbons and nitrogens as an offset in the observed chemical shift following alignment of the RNA. Here, care has to be taken to account for any changes in chemical shift arising from interactions with the ordering medium.[114,116–118] Rather than report on the orientation of the axially symmetric inter-nuclear bond vector relative to a molecular frame, RCSAs report on the orientation of the typically asymmetric chemical shift anisotropy (CSA) tensor centered at a given nucleus (typically nucleobase ^{13}C and ^{15}N and backbone ^{31}P).[87,114,118–120] Because the CSA of protonated nucleobase carbons and nitrogens are often non-coincident with the C–H and N–H bonds, RCSAs can provide independent orientation

information. Moreover, unlike axially symmetric RDCs, asymmetric RCSAs are sensitive to rotations along the CSA principal direction, making them in principle more sensitive spatial probe of structure and dynamics. Methods to fully harness this sensitivity in studies of dynamics remain to be fully established.

9.5 Dynamic Interpretation of RDCs Measured in RNA

9.5.1 Dynamics Information Contained Within RDCs

To appreciate the full angular dynamic information contained within RDCs, it is useful to use a spherical tensor representation to express the measured time-averaged dipolar tensor element $\langle D_0^2 \rangle$ in terms of the overall alignment tensor, O_m^2, of the molecule and 5 out of 25 time-averaged Wigner rotation elements, $\langle D_{n0}^2(\beta\gamma) \rangle$ [Figure 9.4(A)]. These elements are functions of the Euler angles $(\beta\gamma)$ describing the orientation of the bond vector relative to the molecular frame:[27,71,121]

$$\langle D_0^2 \rangle^l = \sum_{m=-2}^{2} \sum_{n=-2}^{2} O_m^2(\mathrm{PAS})^l D_{mn}^2(\theta_l) \langle D_{n0}^2(\beta\gamma) \rangle \tag{6}$$

Here, $O_m^2(\mathrm{PAS})^l$ are elements of the l^{th} overall order/alignment tensor describing averaging of the dipolar interaction due to overall motions expressed in the PAS of the tensor. $D_{mn}^2(\theta_l)$ are elements of a time-independent Wigner rotation matrix that transform the PAS of the l^{th} overall tensor into a common molecular frame. Importantly, eqn (6) assumes that the internal and overall motions of the molecule are uncorrelated to one another.

The information regarding internal motions is contained within the five time-average Wigner elements $\langle D_{nk}^2(\alpha\beta\gamma) \rangle$ ($\{n\} = -2, -1, 0, 1, 2$) which are trigonometric functions of two Euler angles describing the orientation of the bond vector relative to the chiral frame (Table 9.3). The five time-averaged Wigner elements can be determined experimentally for each bond vector provided the measurement of RDCs under five linearly independent alignment conditions, as shown elegantly by Griesinger and Tolman.[26,28] Like the overall order tensor, these five Wigner elements—like the overall order tensor, can be parameterised into an alignment/order tensor, except in this case, the tensor describes the internal dynamics of the axially symmetric RDC bond vector (as opposed to the magnetic field direction) relative to a chiral molecular frame.[26,28,71] The five parameters specify the average orientation of the bond vector relative to the chiral frame, the amplitude of any internal motions, as well as the extent and direction of motional asymmetry. Note that due to the inherent axial symmetry of the dipolar interaction, there is no sensitivity to internal motions that lead to rotations about the bond vector itself (α), therefore limiting sensitivity to only two of the three Euler angles [eqn (6)].

Table 9.3 Elements of the second rank Wigner rotation matrix $D^2_{nk}(\alpha\beta\gamma)$.

n/k	*2*	*1*	*0*	*−1*	*−2*
2	$e^{i2(\alpha+\gamma)}\cos^4\frac{\beta}{2}$	$e^{i(2\gamma+\alpha)}\sin\beta\cos^2\frac{\beta}{2}$	$e^{i2\gamma}\sqrt{\frac{3}{8}}\sin^2\beta$	$e^{i(2\gamma+\alpha)}\sin\beta\sin^2\frac{\beta}{2}$	$e^{i2(\gamma-\alpha)}\sin^4\frac{\beta}{2}$
1	$-e^{i(\gamma+2\alpha)}\sin\beta\cos^2\left(\frac{\beta}{2}\right)$	$e^{i(\gamma+\alpha)}\cos\frac{3\beta}{2}\cos\frac{\beta}{2}$	$e^{i\gamma}\sqrt{\frac{3}{8}}\sin 2\beta$	$e^{i(\gamma-\alpha)}\sin\frac{3\beta}{2}\sin\frac{\beta}{2}$	$e^{i(\gamma-2\alpha)}\sin\beta\sin^2\frac{\beta}{2}$
0	$e^{i2\alpha}\sqrt{\frac{3}{8}}\sin^2\beta$	$-e^{i\alpha}\sqrt{\frac{3}{8}}\sin 2\beta$	$\frac{1}{2}(3\cos^2\beta-1)$	$e^{-i\alpha}\sqrt{\frac{3}{8}}\sin 2\beta$	$e^{-i2\alpha}\sqrt{\frac{3}{8}}\sin^2\beta$
−1	$-e^{i(-\gamma+2\alpha)}\sin\beta\sin^2\left(\frac{\beta}{2}\right)$	$e^{i(-\gamma+\alpha)}\sin\frac{3\beta}{2}\sin\frac{\beta}{2}$	$-e^{-i\gamma}\sqrt{\frac{3}{8}}\sin 2\beta$	$e^{i(-\gamma-\alpha)}\cos\frac{3\beta}{2}\cos\frac{\beta}{2}$	$e^{i(-\gamma-2\alpha)}\sin\beta\cos^2\frac{\beta}{2}$
−2	$e^{i2(-\gamma+\alpha)}\sin^4\frac{\beta}{2}$	$-e^{i(-2\gamma+\alpha)}\sin\beta\sin^2\left(\frac{\beta}{2}\right)$	$e^{-i2\gamma}\sqrt{\frac{3}{8}}\sin^2\beta$	$-e^{i(-2\gamma-\alpha)}\sin\beta\cos^2\left(\frac{\beta}{2}\right)$	$e^{i2(-\gamma-\alpha)}\cos^4\frac{\beta}{2}$

The bond-vector-type analysis of RDCs has been successfully applied to proteins[24,26,28,50,51,80] but has yet to be applied to nucleic acids. Such applications are challenging because of the difficulty in varying the overall alignment of nucleic acids; additionally, it is generally more difficult to measure the required number of spatially independent RDCs to simultaneously determine both internal and overall tensor parameters. As mentioned above, this type of analysis also assumes that internal and overall motions are not correlated to one another, which does not always hold in highly flexible RNA molecules, although domain elongation approaches overcome this problem[71] (see Section 9.5.2).

In principle, much more dynamics information can be obtained from analysing collections of five or more spatially independent RDCs measured in a semi-rigid chiral fragment, such as an A-form helix in RNA.[122,123] Here, one can use the RDCs to determine all five elements of a time-averaged order tensor $\langle T_k^2 \rangle^l$ [Figure 9.4(A)] describing the alignment of a fragment relative to the magnetic field, which can in turn be expressed in terms of the overall alignment tensor of the molecule and time-averaged Wigner rotation elements, $\langle D_{nk}^2(\alpha\beta\gamma) \rangle$:[29]

$$\langle T_k^2 \rangle^l = \sum_{m=-2}^{2} \sum_{n=-2}^{2} O_m^2(\mathrm{PAS})^l D_{mn}^2(\theta_l) \langle D_{nk}^2(\alpha\beta\gamma) \rangle \tag{7}$$

Here, all 25 $\langle D_{nk}^2(\alpha\beta\gamma) \rangle (\{n,k\} = -2, -1, 0, 1, 2)$ time-averaged Wigner elements (Table 9.3) can theoretically be determined, provided the measurement of RDCs and the five elements of $\langle T_k^2 \rangle^l$ under five linearly independent alignment conditions.[29] These 25 time-averaged Wigner elements represent the theoretical maximum dynamic angular information due to internal motions that can be obtained from RDCs.[29] Here, the sensitivity extends to all three Euler angles, including α, as well as co-variations between them, given the simultaneous dependence of many Wigner terms on all three Euler angles.[29,71] The above approach is well suited to analysing RNA chiral helices and 9 out of 25 Wigner elements have been experimentally determined in the TAR RNA system by using the domain elongation strategy.[71] The measurement of all 25 Wigner elements in RNA remains to be an important challenge for the future which will require robust methods for varying alignment.

9.5.2 Decoupling Internal and Overall Motions by Domain Elongation

As described above, the interpretation of RDCs in terms of internal motions often hinges on the assumption that the internal and overall motions are not correlated to one another. This makes it possible to separate averaging contributions due to internal motions from the much larger effects arising due to overall motions.[23,50,58] Indeed, most formalisms developed in studies of protein dynamics invoke this so-called 'decoupling approximation'. In

practice, this decoupling approximation can break down in highly flexible RNA systems. Here, collective motions of A-form helical domains about flexible junctions can lead to large changes in the overall structure of the molecule, and therefore, its overall alignment [Figure 9.4(B)].[71,121,124–126]

A domain elongation strategy has been developed to decouple internal and overall motions in RNA.[71,127] Here, a given helix in a target RNA is elongated, typically by a stretch of 22 base pairs, in order to dominate the overall shape of the molecule, and therefore, its overall alignment, in ordering media or when under the influence of the magnetic field [Figure 9.4(B)]. In this manner, internal motions occurring elsewhere in the molecule have a small effect on the overall shape and therefore alignment of the molecule. The elongated helix is not tagged onto the molecule, where tagging can give rise to complications due to mobility between the tag and target molecule. Rather, it is rigidly integrated within the natural framework of the molecule. To minimise resonance overlap the elongation can be rendered 'NMR invisible' by using an alternating 'GC/CG' elongated helix and A/U labeling or *vice versa* [Figure 9.4(B)].[71,128]

The elongation also has other benefits. To a very good approximation, the elongated helix can be assumed to have an idealised A-form helical geometry. This makes it relatively straightforward to determine the overall alignment of the RNA by using RDCs measured in the elongated helix.[129] Protocols have

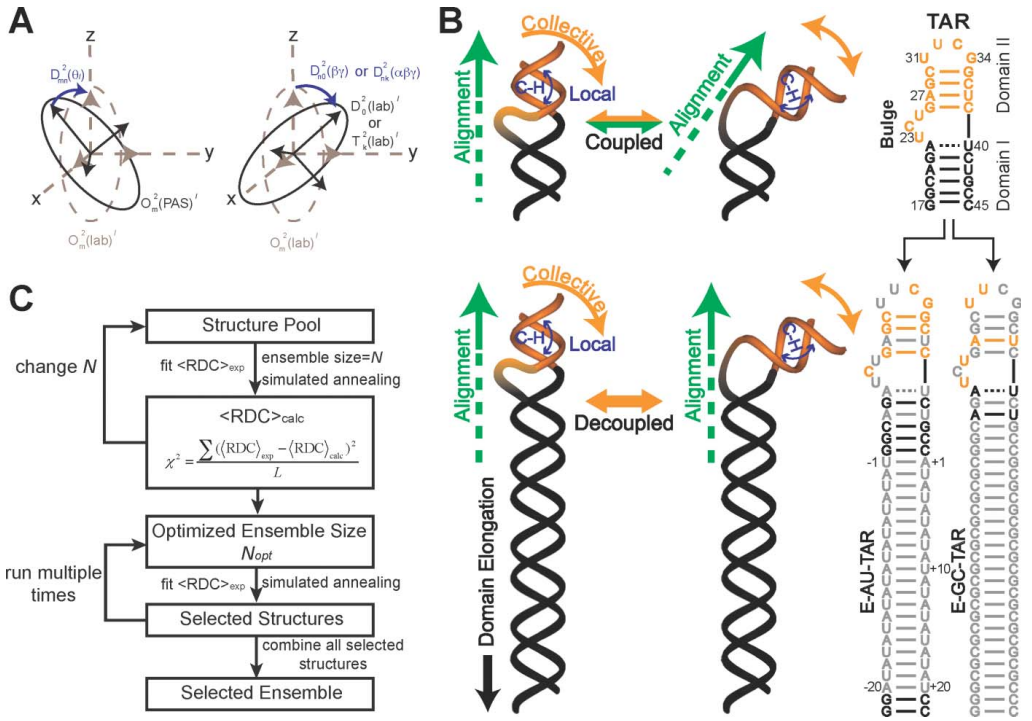

Figure 9.4 Dynamic interpretation of RDCs. (A) Molecular frames and rotations used in the analytical treatment of motions and their impact on RDC observables. (B) Domain-elongation as a strategy for decoupling internal and overall motions. (C) Flowchart for RDC-directed construction of RNA dynamic ensembles using the sample and select (SAS) approach.[1,2]

been developed that allow accurate estimation of any uncertainty in the overall alignment tensor arising due to A-form structural noise and RDC measurement uncertainty.[122] With the overall alignment tensor in hand, the dynamic interpretation of RDCs measured in other parts of the RNA is significantly simplified. Second, by changing which helix is elongated, one can collect independent sets of RDCs that allow measurement of the same motion from a different molecule-centered perspective.[71] This makes it possible to measure a large number of the underlying time-averaged Wigner elements [eqn (7)] and thereby characterise motions with greater spatial resolution. For systems composed of more than two helices, correlated motions between helical domains can be characterised.[29] For simple hairpin structures, modulating the length of elongation can be sufficient to modulate the alignment of the RNA molecule.[78]

9.5.3 Inter-Helical Motions from Order Tensor Analysis of RDCs

Many regulatory RNA molecules undergo conformational transitions involving large changes in the relative orientation of A-form helical domains about flexible junctions that typically contain residues that are key for protein/ligand recognition and/or catalysis. This has spurred the development of RDC methods directed specifically at determining the orientation and dynamics of helical domains in RNA.

A qualitative framework based on the order tensor analysis of RDCs developed originally to characterise fragment orientation and dynamics in proteins[130,131] has been applied to characterise inter-helical motions in RNA. In this approach, more than five independent RDCs are used to determine five order tensor elements describing partial alignment of each helix relative to the magnetic field. Here, regions of the helices that consist of two or more non-terminal contiguous hydrogen-bonded Watson–Crick (WC) base pairs are modelled assuming a standard canonical A-form helix geometry by building sequence-specific helices using RNA structure-prediction programs.[97,122,123] These WC pairs can be experimentally verified using *trans*-hydrogen bond J_{NN}-COSY-type NMR experiments for directly detecting N–H–N hydrogen bonds.[94,132] Note that WC pairs flanked by GU pairs or non-canonical motifs can also be used, although higher levels of structure/dynamic noise need to be considered in the analysis.[122] Any uncertainty arising from the assumed canonical A-form helix geometry (referred to as 'structural noise'[133]) is propagated into the order tensor parameters and ultimately the relative orientation and dynamics of helices. In particular, the effects of A-form structural noise as well as RDC measurement uncertainty can be taken into account in the determination of order tensors using the program AFORM-RDC.[122] Other more general approaches for dealing with structural noise in the determination of alignment tensors have also been described.[133]

The order tensor describes the average alignment of each helix relative to the applied magnetic field. For elongated RNA molecules, the magnetic field

direction is approximately anchored along the axially symmetric axis of the elongated helix [Figure 9.4(B)]. The average orientation of fragments—one relative to the other—can be obtained by superimposing their order tensor frames.[59,60,134] The latter amounts to insisting that helical fragments share, on average, a common view of the magnetic field direction when assembled into a proper structure—similar to how countries in a properly assembled map report to a common compass bearing. The five independent parameters of the order tensor can be compared for various helices to obtain information about relative helix motions over sub-millisecond timescales.[59] While helices will report identical parameters when they are held rigid relative to one another, inter-helix motions can lead to differences. Specifically, the ϑ value for a given helix will be attenuated relative to the value observed for a helix that more strongly dominates total alignment, with the degree of attenuation generally increasing with motional amplitudes. By taking the ratio of the ϑ values for each helix (ϑ_{HI} /ϑ_{HII} = ϑ_{int}), where ϑ_{int} ranges from 0 to 1 with 0 having maximum and 1 having minimum motions, the degree of internal motions can be determined. Although often difficult to determine reliably, the asymmetry parameter (η) can provide insight into the directionality of inter-helix motions with spatially isotropic (directionless) motions having a smaller effect on the relative helix η values compared to anisotropic (directional) motions.[59,135]

Order tensor analysis of RDCs assumes that one fragment dominates overall molecular alignment of the RNA.[59,85,135,136] As discussed above, this 'decoupling limit' is readily satisfied in elongated RNA molecules or when helices are held rigidly together. Two other regimes can be identified. In the extreme coupling limit, helices have similar size and shape and contribute equally to overall alignment. Here, similar degrees of order may be observed, even in the presence of inter-helical motions, and the observation of $\vartheta_{int} = 1$ does not rule out the presence of inter-helix motions. Note that depending on the nature of inter-helical motional trajectory, different ϑ values may be observed even if the helices have equivalent size and shape. For example, twisting around the axis of a given helix will result in a reduction of its ϑ without affecting the ϑ value observed in an adjoining helix. In the intermediate coupling limit, one helix partially dominates overall alignment and the measured ϑ_{int} value will underestimate the real motional amplitudes.[137] Note that differences on the order of three base pairs can be sufficient to take an RNA system outside the extreme coupling limit and into the intermediate regime.[78]

9.5.4 Constructing Dynamic Ensembles

Another approach for obtaining atomic-level information regarding RNA dynamics involves using RDCs to construct dynamic structure ensembles. This was first demonstrated by Clore and co-workers who analysed RDCs measured in ubiquitin to create a two-state ensemble[138] and then subsequently applied the same approach in the determination of a four-state ensemble of

DNA.[139] Alternatively, approaches have been developed in which RDCs are used to guide selection of conformers from a conformational pool generated by molecular dynamics (MD) simulations[30,32] or corresponding to an exhaustive set of allowed conformations.[71,140]

The ability to construct dynamic ensembles using RDCs relies on being able to compute RDCs for a given candidate conformer on the basis of its structure. This, in turn, requires a means for determining the overall tensor of the molecule. Domain elongation provides a simple solution to this otherwise potentially intractable problem, given that the overall tensor of a non-elongated RNA molecule may vary from molecule to molecule in a manner that is difficult to measure experimentally or predict computationally.[129] In elongated RNA molecules, the overall tensor of the RNA can be determined by analysing RDCs measured in the elongated helix. Because the elongated helix dominates the overall structure, internal motions in different parts of the RNA molecule are less likely to modulate the overall tensor. Thus, the overall tensor determined for the elongated helix can be used to predict RDCs for any arbitrary structure and time-averaged RDCs can be determined for a given MD trajectory or a candidate ensemble of conformations.[129].

Although there are sparse examples of using RDCs to probe DNA dynamics, one of the earliest RDC ensembles was constructed for DNA.[139] Clore and co-workers performed structure refinement on the model Dickerson dodecamer against X-ray and NMR structures, X-ray scattering, CSA, and RDC data. The incorporation of P-H3′ RDC and CSA data fitted poorly to existing structures, and only fitted well when a four-state ensemble was allowed, demonstrating anisotropic motion within the DNA backbone. The derived ensemble showed significant deviations from idealised B-form geometry, with large amplitude tilt and propeller twist motions (9–18° and 15–30°, respectively).[139]

Another approach for constructing ensembles uses RDCs to guide the selection of RNA conformers from a pool containing thousands of conformers.[141–144] First, the agreement between experimentally measured RDCs and values computed from the entire pool of conformations, such as an MD trajectory, is evaluated. For example, in the case of HIV-1 TAR, the measured RDCs agreed poorly with those computed from an 80 nanosecond MD simulation (RMSD = 15.1 Hz compared to experimental error of $\sim$4 Hz).[16] This disagreement may reflect deficiencies in the force field, but it may also reflect lack of convergence, given that the RDC timescale sensitivity extends well beyond 80 nanoseconds into the millisecond time regime. To construct an ensemble describing the experimental data, a 'Sample and Select' method was implemented, operating as follows [Figure 9.4(C)].[141] Sub-ensembles with increasing size are constructed in an attempt to find the smallest member ensemble (N) satisfying the measured RDCs. Here, N conformers are randomly selected from the pool and the agreement between measured and predicted RDCs is computed. Next, one of the chosen conformers is replaced randomly with another conformer from the pool, and

the agreement with measured RDCs is re-examined and the newly selected conformer is either accepted or rejected based on the metropolis criteria [Figure 9.4(C)]. Using such a Monte Carlo based approach, several iterations are carried out until convergence is reached, defined as achieving agreement with the measured RDCs exceeding the experimental error. The ensemble size is then incrementally increased in steps of 1 from $N = 1$ until convergence is reached. Using this approach, with a starting MD-generated conformation pool of 80 000 TAR structures, an ensemble of 20 conformers was determined that agreed to near-within experimental error with measured RDCs (RMSD = 4.8 Hz compared to experimental error $\sim$4 Hz).[16]

Approaches have also been developed to use RDCs in reconstructing smooth continuous motional paths.[140] In one approach, the time-averaged Wigner elements are expressed in terms of a four-dimensional quaternion $q(u)$ representing the relative orientation of two chiral fragments as a single-axis rotation from which a four-dimensional hypersphere can be defined. On this hypersphere, the quaternion can be further expressed as a line integral over a curve in configuration space which contains a heterogeneous ensemble of equally weighted conformations. The curve is approximated using a series of geodesic segments, and the resultant weights of different conformations are proportional to the number of times the path visits that particular conformation. With this approach, the authors showed that the measurement of RDCs under five alignment conditions can be used to reconstruct salient features of a multi-segment inter-helical motional trajectory corresponding to an MD simulation of TAR RNA.[140]

It is important—and often not trivial—to independently assess any dynamic ensemble or motional model generated using RDCs. Several strategies can be used. First, part of the RDC data can be omitted from the dynamics analysis and reserved until the end to evaluate the constructed dynamics.[86,145,146] However, care should be taken in selecting which RDCs to exclude and ensuring that they correspond to regions that have other RDCs to help define structural dynamics. One could use an independent set of RDCs, such as those that can be obtained using field-induced alignment and for which the overall χ-tensor for a given candidate conformer can be predicted based on structure.[121] Second, the constructed dynamics can be interrogated with other NMR measurements, including NOEs and NMR probes of hydrogen bonding. For example, in the analysis of the generated TAR dynamic ensemble, the flexible bulge residue U23 is frequently stacked on helical residue A22, consistent with an NOE cross-peak observed between these two bases, and the flexible A22-U40 base pair rarely formed the expected WC hydrogen bond geometry, consistent with the severe line broadening of the U40 imino proton.[16]

9.5.5 Explicit Treatment of Motional Couplings

All of the above approaches assume that the internal and overall motions are not correlated to one another. What happens when this approximation breaks

down? Considering such correlations requires the ability to predict the overall alignment/order tensor based on the structure of an RNA conformer. As mentioned above, one case in which this is feasible is magnetic-field-induced alignment. Here, the overall χ-tensor can be predicted for a given RNA conformer based on a tensor summation over all χ-tensors associated with individual nucleobases.[52,85,121] Furthermore, one can write expressions relating the overall χ-tensor in terms of the χ-tensors of individual helices and their relative orientation. By taking advantage of this simple relationship, Zhang and co-workers showed that couplings between inter-helical motions and the overall alignment can be explicitly treated in the case of magnetic field alignment.[121] This study revealed that RDCs measured in the presence of motional couplings, in fact, carry greater information regarding the underlying dynamics compared to RDCs measured under the decoupling limit. This provides great motivation to apply approaches for predicting overall alignment in ordering media in the dynamic analysis of RDCs measured in RNA. Though several studies have shown that the alignment of RNA in phage can be accurately computed based on the RNA structure, further benchmark studies are required to establish the accuracy of such predictions under a range of ionic strength conditions and for a variety of RNA tertiary contexts.

9.6 Example Applications in Studies of RNA Dynamics From RDCs

The application of RDCs in studies of RNA dynamics has yielded fundamental new insights into the dynamic behavior of RNA. Many early studies identified dynamic hot-spots as regions with RDCs that could not readily be satisfied using a single static structure.[23] Many of these residues were localised within flexible junctions that tether helices together and in many cases, independent evidence for flexibility could be obtained based on measurements of spin relaxation data.

An early example is a study by Sibille and co-workers which used RDCs and MD simulations to refine the global and local structure of the theophylline-binding RNA aptamer-ligand complex from an existing NOE-based NMR structure.[147] The inclusion of RDCs measured in the nucleobase of a flexible internal loop residue C27 in the structure refinement resulted in several different conformations for this residue suggesting a contribution from motional averaging[147] [Figure 9.5(A)]. In other studies, dynamic hot-spots were identified by examining the fit of measured RDCs to a known X-ray structure of the RNA. For example, deviations between RDCs measured in the unbound 84-nt guanine riboswitch and values predicted from an X-ray structure of the ligand-bound form were observed for a sub-set of residues that form the binding pocket, indicating that while the overall riboswitch structure is preformed, the binding pocket is locally disordered.[148]

RDCs have also provided fundamental insights into global motions involving the collective movements of helical elements. Some of the earliest

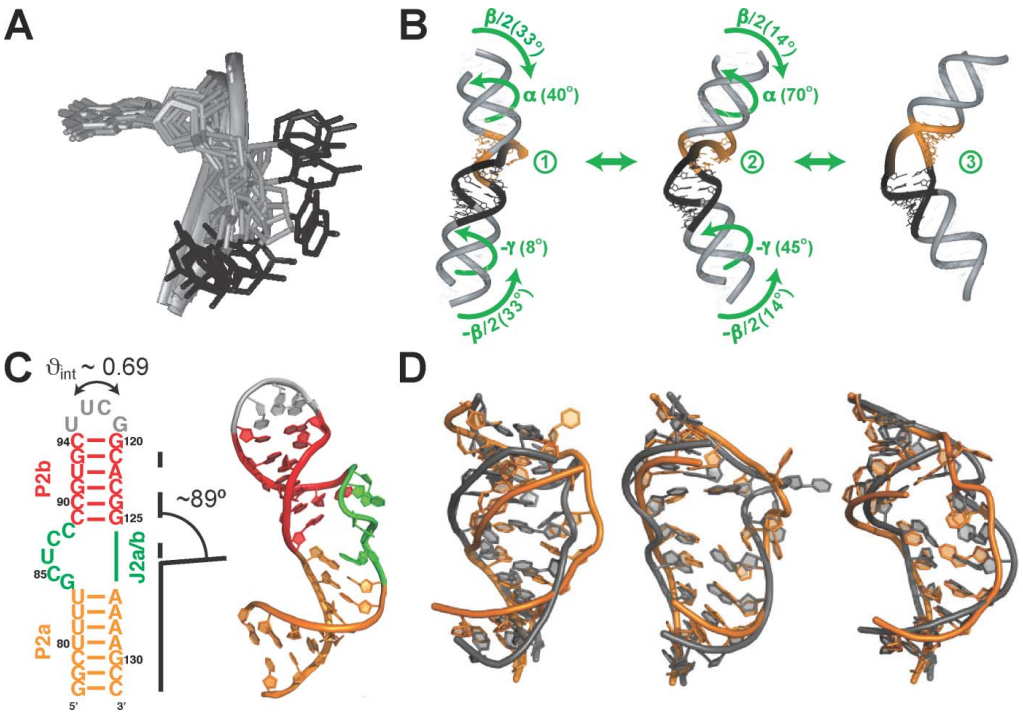

Figure 9.5 Application of RDCs in the analysis of RNA dynamics. (A) RDC-derived local motions of a bulge xx or intern loop xx residue C27 (black) in theophylline–RNA complex. Reproduced from ref. [147] with permission. © American Chemical Society, 2001. (B) Global motions observed using RDCs involving correlated changes in the inter-helical twist (α and γ) and bend (β) angles. Reproduced from ref. [71] with permission. (C) Secondary structure (left) and NMR structure of human telomerase P2ab (PDB ID 2L3E, right). Superposition of the order tensor frames yields an average inter-helical angle of 89°, and internal generalised degree of order ϑ_{int} ~0.69 (where ϑ_{int} ranges from 0–1, with 0 being flexible and 1 being rigid). (D) Conformers from atomic-resolution dynamics ensemble of HIV-1 TAR (grey) constructed by combining domain-elongation RDCs and molecular dynamics simulations reveals very high similarity to those observed in ligand bound states (orange). Reproduced with permission from ref. 16. 1

applications of RDCs to RNA provided evidence for large-amplitude (~45°) collective inter-helical motions in HIV-1 TAR RNA that occur about a flexible trinucleotide bulge.[127,149] Discrete ensemble analysis of RDCs measured in two domain elongated TAR RNA constructs [Figure 9.4(B)] made it possible to visualise the inter-helical trajectory in 3D. Results revealed a specific trajectory in which the helices bend and twist in a spatially correlated manner[71] [Figure 9.5(B)]. Thus, while the helices undergo large amplitude collective motions (>90°), they do not move in a spatially random manner. Importantly, all of the known ligand-bound TAR conformations fall along various positions of this dynamic trajectory, indicating that ligands most likely capture pre-existing TAR conformations by 'conformational selection'. It is important to note that the inter-helical motions observed in TAR using RDCs are not fully

captured by spin relaxation data, most likely because the motions occur at the nano- to microsecond timescale that are inaccessible to spin relaxation.[127,150]

A subsequent survey of RNA junctions in the Protein Data Bank (PDB) together with molecular modeling revealed that the inter-helical trajectory observed for TAR using RDCs is a fundamental and universal dynamic feature of two-way junctions. The specific motional trajectory arises from simple connectivity and steric constraints that restrict the allowed orientation of helices along specific pathways.[151,152] These constraints were placed on a quantitative footing and shown to provide the basis for the spatially correlated twisting motions observed between two helices in HIV-1 TAR.[152] These topological constraints—uncovered with the aid of RDCs—provide a blueprint for quantitatively understanding RNA inter-helical motions across a variety of junctions.[153]

RDC studies, many targeting the TAR model system, have provided insights into the dependence of inter-helical motions on various parameters of interest. For example, different small molecules bind TAR and arrest the inter-helical motions as well as induce co-axial stacking by variable amounts that appear dependent on the number of cationic groups in the small molecule.[71,154,155] Likewise, increasing the concentration of Mg^{2+} or Na^{+} leads to the arrest of TAR inter-helical motions and stabilisation of a co-axially stacked conformation.[156] These studies suggest that co-axial stacking of helices is likely unfavorable due to negative charge repulsion, which accumulates at the structurally confined bulge, and that interactions with cationic groups and counterions may help alleviate this unfavorable charge repulsion. Reducing the length of the TAR bulge linker from three to two nucleotides also resulted in the expected reduction in the amplitude of inter-helical motions and stabilisation of a more co-axial TAR conformation.[71]

However, the dependence of inter-helical motions on bulge linker is not always trivial. For example, Zhang and co-workers used an order tensor analysis of RDCs to measure inter-helical motions across the five-nucleotide bulge in the core domain of human telomerase RNA.[157] Their results revealed surprisingly smaller amplitude inter-helical motions than those observed across the shorter TAR trinucleotide bulge [Figure 9.5(C)]. Here, unique stacking of the guanine within the bulge over to the far-removed strand may serve to lock the inter-helical structure and reduce the amplitude of inter-helical motions observed. RDC studies are also revealing that the amplitude of inter-helical motions can depend on the sequence of WC base pairs flanking junctions. For example, Stelzer *et al.* rationally re-engineered TAR to bias the dynamic ensemble towards the ligand-bound co-axial conformation. This was accomplished by swapping an AU base pair with a GC base pair below the bulge, which is expected to more favorably stack with the GC base pair in the adjacent helix.[155] By pre-stabilising the ligand-bound state, the mutant bound argininamide with three-fold higher affinity.

By combining domain elongation RDCs with MD simulations, Frank *et al.* determined an atomic resolution dynamic ensemble for the 3-nt bulge and the

2-nt bulge of HIV-1 and HIV-2 TAR RNA, respectively.[16] The authors found that snapshots within the dynamic ensemble closely matched ligand-bound conformations of TAR, further supporting that adaptive recognition may proceed *via* 'conformational selection' [Figure 9.5(D)]. Comparison of the HIV-1 and HIV-2 TAR dynamic ensembles revealed that reducing the length of the bulge leads to a significant reduction in local motions of the A22-U40 junctional base pair and bulge residues U23 and U25, and this ordering likely drives the reduction in the amplitude of inter-helical motions. The ensemble revealed that the WC base pairs within A-form helices adopt a stable geometry consistent with an idealised A-form helix structure.

More recently, the RDC-derived TAR dynamics ensemble was subjected to computational screening.[15] This provided one avenue for overcoming the difficulty in computationally modeling changes in RNA structure that take place on small molecule binding and resulted in the *de novo* discovery of six small molecules that bind TAR, one of which inhibited HIV replication in T-cell lines *in vivo* with an IC_{50} of $\sim$20 μM.[15] Thus, RDC studies of RNA dynamics are already being translated into important biomedical applications.

RDCs have also been used to characterise the dynamic and structural characteristics of highly flexible single-stranded RNA. By combining spin relaxation measurements and MD simulations, Eichhorn and co-workers were able to show that the 12-nt adenine-rich single-stranded tail derived from the prequeuosine riboswitch maintained a high degree of order in the polyadenine core, despite a high level of internal dynamics. RDCs fit extremely well to an A-form helix, suggesting rapid exchange between an isotropically unfolded and stacked, A-form-like conformation.[72] These studies suggest that RDCs may provide the much-needed experimental parameters needed to characterise the poorly understood conformation of highly disordered single-stranded RNA—the RNA equivalent of intrinsically disordered proteins.

9.7 Summary and Future Perspectives

Methods for measuring and interpreting RDCs in terms of RNA dynamics have matured significantly over the past five years and can now be applied broadly to study the dynamic properties of RNA structure. There are nevertheless still some key areas that will require further developments in the future. First, robust approaches for varying RNA alignment need to be developed in order to extract the full dynamics information contained within RDCs. Second, more practical approaches need to be developed to measure RDCs of the sugar and phosphodiester backbone. Third, the application of RDC dispersion, as implemented for proteins,[158–160] should enable the characterisation of transient structures of nucleic acids and open an entirely new direction of RDC-driven dynamics studies. Finally, methods must continue to be devised to combine RDCs with additional experimental measurements and computational techniques—only then will it be possible to unravel the dazzling complexity of RNA dynamics.

Thus far, RDC studies of RNA dynamics have mostly focused on model systems. This has proven to be quite fruitful, resulting in the discovery of general principles that apply widely across a wide range of RNA structures. In particular, a great deal of information has been obtained regarding the dependence of inter-helical motions on RNA secondary structure as well as external factors such as ligands and metals. The generality of these findings has to be examined by investigating structurally and functionally distinct RNA molecules—including RNA containing three-way and higher order junctions. Studies must also target larger more complex RNA architectures and explore other modes of motion, such as base-flipping and changes in hydrogen bond alignments. We hope that this chapter will help enable some of these future applications.

Acknowledgements

We thank members of the Al-Hashimi lab for insightful comments and Dr. Alex Kurochkin for his expertise and maintenance of the NMR instruments. H. M. A. would like to acknowledge fruitful collaborations with the groups of Carol Fierke (University of Michigan), Charles L. Brooks III (University of Michigan), and Ioan Andricioaei (University of California – Irvine). The authors gratefully acknowledge the Michigan Economic Development Cooperation and the Michigan Technology Tri-Corridor for support in the purchase of the 600 MHz spectrometer. This work was supported by the National Institutes of Health (RO1 AI066975-01 and RO1-GM089846) and a National Science Foundation CAREER award (MCB 0644278).

References

1. V. Ambros, *Nature*, 2004, **431**, 350–355.
2. L. He and G. J. Hannon, *Nat. Rev. Genet.*, 2004, **5**, 522–531.
3. J. S. Mattick, *Nat. Rev. Genet.*, 2004, **5**, 316–323.
4. C. C. Mello and D. Conte Jr, *Nature*, 2004, **431**, 338–342.
5. H. Frauenfelder, S. G. Sligar and P. G. Wolynes, *Science*, 1991, **254**, 1598–1603.
6. H. M. Al-Hashimi and N. G. Walter, *Curr. Opin. Struct. Biol.*, 2008, **18**, 321–329.
7. J. A. Cruz and E. Westhof, *Cell*, 2009, **136**, 604–609.
8. E. A. Dethoff, J. Chugh, A. M. Mustoe and H. M. Al-Hashimi, *Nature*, 2011, in press. 2
9. N. Leulliot and G. Varani, *Biochemistry*, 2001, **40**, 7947–7956.
10. K. F. Blount and R. R. Breaker, *Nat. Biotechnol.*, 2006, **24**, 1558–1564.
11. R. Micura and C. Hobartner, *ChemBioChem*, 2003, **4**, 984–990.
12. T. A. Cooper, L. Wan and G. Dreyfuss, *Cell*, 2009, **136**, 777–793.
13. T. Hermann, *Biochimie*, 2002, **84**, 869–875.
14. S. Fulle and H. Gohlke, *J. Mol. Recognit.*, 2010, **23**, 220–231.

15. A. C. Stelzer, A. T. Frank, J. D. Kratz, M. D. Swanson, M. J. Gonzalez-Hernandez, J. Lee, I. Andricioaei, D. M. Markovitz and H. M. Al-Hashimi, *Nat. Chem. Biol.*, 2011, **7**, 553–559.
16. A. T. Frank, A. C. Stelzer, H. M. Al-Hashimi and I. Andricioaei, *Nucleic Acids Res.*, 2009, **37**, 3670–3679.
17. P. Banas, D. Hollas, M. Zgarbova, P. Jurecka, M. Orozco, T. E. Cheatham, J. Sponer and M. Otyepka, *J. Chem. Theory Comput.*, 2010, **6**, 3836–3849.
18. J. R. Bothe, E. N. Nikolova, C. D. Eichhorn, J. Chugh, A. L. Hansen and H. M. Al-Hashimi, *Nat. Methods*, 2011, **8**, 919–931.
19. J. Rinnenthal, J. Buck, J. Ferner, A. Wacker, B. Furtig and H. Schwalbe, *Acc. Chem. Res.*, 2011.
20. J. R. Tolman, J. M. Flanagan, M. A. Kennedy and J. H. Prestegard, *Proc. Natl. Acad. Sci. U. S. A.*, 1995, **92**, 9279–9283.
21. N. Tjandra and A. Bax, *Science*, 1997, **278**, 1111–1114.
22. J. R. Tolman, J. M. Flanagan, M. A. Kennedy and J. H. Prestegard, *Nat. Struct. Biol.*, 1997, **4**, 292–297.
23. M. Getz, X. Sun, A. Casiano-Negroni, Q. Zhang and H. M. Al-Hashimi, *Biopolymers*, 2007, **86**, 384–402.
24. B. E. Ramirez and A. Bax, *J. Am. Chem. Soc.*, 1998, **120**, 9106–9107.
25. H. M. Al-Hashimi, H. Valafar, M. Terrell, E. R. Zartler, M. K. Eidsness and J. H. Prestegard, *J. Magn. Reson.*, 2000, **143**, 402–406.
26. J. R. Tolman, *J. Am. Chem. Soc.*, 2002, **124**, 12020–12030.
27. J. Meiler, J. J. Prompers, W. Peti, C. Griesinger and R. Bruschweiler, *J. Am. Chem. Soc.*, 2001, **123**, 6098–6107.
28. W. Peti, J. Meiler, R. Bruschweiler and C. Griesinger, *J. Am. Chem. Soc.*, 2002, **124**, 5822–5833.
29. C. K. Fisher, Q. Zhang, A. Stelzer and H. M. Al-Hashimi, *J. Phys. Chem. B*, 2008, **112**, 16815–16822.
30. D. MacDonald and P. Lu, *Curr. Opin. Struct. Biol.*, 2002, **12**, 337–343.
31. S. A. McCallum and A. Pardi, *J. Mol. Biol.*, 2003, **326**, 1037–1050.
32. M. P. Latham, D. J. Brown, S. A. McCallum and A. Pardi, *ChemBioChem*, 2005, **6**, 1492–1505.
33. A. Grishaev, J. Ying, M. D. Canny, A. Pardi and A. Bax, *J. Biomol. NMR*, 2008, **42**, 99–109.
34. E. W. Bastiaan and C. MacLean, *NMR: Basic Princ. Prog.*, 1990, **25**, 17–43.
35. E. W. Bastiaan, C. Maclean, P. C. M. Van Zilj and A. A. Bothner-by, *Ann. Rep. NMR Spec.*, 1987, **19**, 35–77.
36. P. Diehl and C. L. Khetrapal, *NMR Studies of Molecules Oriented in the Nematic Phase of Liquid Crystals*, Springer-Verlag, New York, 1969.
37. J. W. Emsley and J. C. Lindon, *NMR Spectroscopy using Liquid Crystal Solvents*, 1st edn, Pergamon Press, Oxford, 1975.
38. C. Gayathri, A. A. Bothnerby, P. C. M. Vanzijl and C. Maclean, *Chem. Phys. Lett.*, 1982, **87**, 192–196.

39. C. L. Khetrapal, A. C. Kunwar, A. G. Tracey and P. Diehl, *Nuclear Magnetic Resonance Studies in Lyotropic Liquid Crystals*, Springer-Verlag, New York, 1975.
40. J. A. B. Lohman and C. MacLean, *Chem. Phys.*, 1978, **35**, 269–274.
41. A. Saupe, *Angew. Chem., Int. Ed. Engl.*, 1968, **7**, 97–112.
42. L. C. Snyder, *J. Chem. Phys.*, 1965, **43**, 4041–&.
43. P. C. M. Vanzijl, B. H. Ruessink, J. Bulthuis and C. Maclean, *Acc. Chem. Res.*, 1984, **17**, 172–180.
44. A. A. Bothner-By, *Encycl. Nucl. Magn. Reson.*, 1995, **5**, 2932–2238.
45. D. MacDonald and P. Lu, *Curr. Opin. Struct. Biol.*, 2002, **12**, 337–343.
46. R. S. Lipsitz and N. Tjandra, *Annu. Rev. Biophys. Biomol. Struct.*, 2004, **33**, 387–413.
47. J. H. Prestegard, C. M. Bougault and A. I. Kishore, *Chem. Rev.*, 2004, **104**, 3519–3540.
48. A. Bax and A. Grishaev, *Curr. Opin. Struct. Biol.*, 2005, **15**, 563–570.
49. M. Blackledge, *Prog. Nucl. Magn. Reson. Spectrosc.*, 2005, **46**, 23–61.
50. J. R. Tolman and K. Ruan, *Chem. Rev.*, 2006, **106**, 1720–1736.
51. J. R. Tolman and H. M. Al-Hashimi, *Ann. Rep. NMR Spectrosc.*, 2003, **51**, 105–166.
52. N. Tjandra, J. G. Omichinski, A. M. Gronenborn, G. M. Clore and A. Bax, *Nat. Struct. Biol.*, 1997, **4**, 732–738.
53. A. Abragam, *The Principles of Nuclear Magnetism*, Clarendon Press, Oxford, 1961.
54. R. R. Ernst, G. Bodenhausen and A. Wokaun, *Principles of Nuclear Magnetic Resonance in One and Two Dimensions*, Clarendon Press, Oxford, 1987.
55. W. D. Cornell, P. Cieplak, C. I. Bayly, I. R. Gould, K. M. Merz, D. M. Ferguson, D. C. Spellmeyer, T. Fox, J. W. Caldwell and P. A. Kollman, *J. Am. Chem. Soc.*, 1995, **117**, 5179 – 5197.
56. L. Clowney, S. C. Jain, A. R. Srinivasan, J. Westbrook, W. K. Olson and H. M. Berman, *J. Am. Chem. Soc.*, 1996, **118**, 509–518.
57. X. P. Xu and D. A. Case, *J. Biomol. NMR*, 2001, **21**, 321–333.
58. L. Salmon, G. Bouvignies, P. Markwick and M. Blackledge, *Biochemistry*, 2011, **50**, 2735–2747.
59. J. R. Tolman, H. M. Al-Hashimi, L. E. Kay and J. H. Prestegard, *J. Am. Chem. Soc.*, 2001, **123**, 1416–1424.
60. J. A. Losonczi, M. Andrec, M. W. Fischer and J. H. Prestegard, *J. Magn. Reson.*, 1999, **138**, 334–342.
61. N. Tjandra, *Struct. Folding Des.*, 1999, **7**, R205–R211.
62. J. H. Prestegard and A. I. Kishore, *Curr. Opin. Chem. Biol.*, 2001, **5**, 584–590.
63. P. Ram and J. H. Prestegard, *Biochim. Biophys. Acta*, 1988, **940**, 289–294.
64. C. R. Sanders, B. J. Hare, K. P. Howard and J. H. Prestegard, *Prog. Nucl. Magn. Reson. Spectrosc.*, 1994, **26**, 421–444.

65. G. M. Clore, M. R. Starich and A. M. Gronenborn, *J. Am. Chem. Soc.*, 1998, **120**, 10571–10572.
66. M. R. Hansen, L. Mueller and A. Pardi, *Nat. Struct. Biol.*, 1998, **5**, 1065–1074.
67. M. R. Hansen, P. Hanson and A. Pardi, *Methods Enzymol.*, 2000, **317**, 220–240.
68. B. Wu, M. Petersen, F. Girard, M. Tessari and S. S. Wijmenga, *J. Biomol. NMR*, 2006, **35**, 103–115.
69. M. Zweckstetter and A. Bax, *J. Biomol. NMR*, 2001, **20**, 365–377.
70. M. Zweckstetter, G. Hummer and A. Bax, *Biophys. J.*, 2004, **86**, 3444–3460.
71. Q. Zhang, A. C. Stelzer, C. K. Fisher and H. M. Al-Hashimi, *Nature*, 2007, **450**, 1263–1267.
72. C. D. Eichhorn, J. Feng, K. C. Suddala, N. G. Walter, C. L. Brooks III and H. M. Al-Hashimi, *Nucleic Acids Res.*, 2011. 3
73. K. Ruan, K. B. Briggman and J. R. Tolman, *J. Biomol. NMR*, 2008, **41**, 61–76.
74. K. Bondensgaard, E. T. Mollova and A. Pardi, *Biochemistry*, 2002, **41**, 11532–11542.
75. M. P. Latham, P. Hanson, D. J. Brown and A. Pardi, *J. Biomol. NMR*, 2008, **40**, 83–94.
76. H. M. Al-Hashimi, A. Gorin, A. Majumdar and D. J. Patel, *J. Am. Chem. Soc.*, 2001, **123**, 3179–3180.
77. J. Ying, A. Grishaev, M. P. Latham, A. Pardi and A. Bax, *J. Biomol. NMR*, 2007, **39**, 91–96.
78. E. A. Dethoff, A. L. Hansen, Q. Zhang and H. M. Al-Hashimi, *J. Magn. Reson.*, 2010, **202**, 117–121.
79. H. C. Kung, K. Y. Wang, I. Goljer and P. H. Bolton, *J. Magn. Reson., Ser. B*, 1995, **109**, 323–325.
80. J. H. Prestegard, J. R. Tolman, H. M. Al-Hashimi and M. Andrec, in *Biological Magnetic Resonance*, ed. N. R. Krishna and L. J. Berliner, Plenum, New York, 1999, vol. 17, pp. 311–355.
81. H. M. Al-Hashimi, A. Majumdar, A. Gorin, A. Kettani, E. Skripkin and D. J. Patel, *J. Am. Chem. Soc.*, 2001, **123**, 633–640.
82. B. N. van Buuren, J. Schleucher, V. Wittmann, C. Griesinger, H. Schwalbe and S. S. Wijmenga, *Angew. Chem., Int. Ed.*, 2004, **43**, 187–192.
83. J. R. Tolman and J. H. Prestegard, *J. Magn. Reson., Ser. B*, 1996, **112**, 245–252.
84. N. Tjandra, S. Grzesiek and A. Bax, *J. Am. Chem. Soc.*, 1996, **118**, 6264–6272.
85. Q. Zhang, R. Throolin, S. W. Pitt, A. Serganov and H. M. Al-Hashimi, *J. Am. Chem. Soc.*, 2003, **125**, 10530–10531.
86. L. Salmon, G. Bouvignies, P. Markwick, N. Lakomek, S. Showalter, D. W. Li, K. Walter, C. Griesinger, R. Bruschweiler and M. Blackledge, *Angew. Chem., Int. Ed.*, 2009, **48**, 4154–4157.

87. J. Ying, A. Grishaev, D. L. Bryce and A. Bax, *J. Am. Chem. Soc.*, 2006, **128**, 11443–11454.
88. M. Ottiger, F. Delaglio and A. Bax, *J. Magn. Reson.*, 1998, **131**, 373–378.
89. L. Zidek, H. Wu, J. Feigon and V. Sklenar, *J. Biomol. NMR*, 2001, **21**, 153–160.
90. P. Permi, *J. Biomol. NMR*, 2002, **22**, 27–35.
91. S. W. Pitt, A. Majumdar, A. Serganov, D. J. Patel and H. M. Al-Hashimi, *J. Mol. Biol.*, 2004, **338**, 7–16.
92. B. Brutscher, J. Boisbouvier, A. Pardi, D. Marion and J. P. Simorre, *J. Am. Chem. Soc.*, 1998, **120**, 11845–11851.
93. K. Pervushin, R. Riek, G. Wider and K. Wuthrich, *J. Am. Chem. Soc.*, 1998, **120**, 6394–6400.
94. K. Pervushin, A. Ono, C. Fernandez, T. Szyperski, M. Kainosho and K. Wüthrich, *Proc. Natl. Acad. Sci. U. S. A.*, 1998, **95**, 14147–14151.
95. R. Fiala, J. Czernek and V. Sklenar, *J. Biomol. NMR*, 2000, **16**, 291–302.
96. J. Boisbouvier, D. L. Bryce, E. O'Neil-Cabello, E. P. Nikonowicz and A. Bax, *J. Biomol. NMR*, 2004, **30**, 287–301.
97. J. Ying, J. Wang, A. Grishaev, P. Yu, Y. X. Wang and A. Bax, *J. Biomol. NMR*, 2011, **51**, 89–103.
98. B. Luy and J. P. Marino, *J. Magn. Reson.*, 2003, **163**, 92–98.
99. B. S. Tolbert, Y. Miyazaki, S. Barton, B. Kinde, P. Starck, R. Singh, A. Bax, D. A. Case and M. F. Summers, *J. Biomol. NMR*, 2010, **47**, 205–219.
100. J. Yan, T. Corpora, P. Pradhan and J. H. Bushweller, *J. Biomol. NMR*, 2002, **22**, 9–20.
101. E. O'Neil-Cabello, D. L. Bryce, E. P. Nikonowicz and A. Bax, *J. Am. Chem. Soc.*, 2004, **126**, 66–67.
102. E. Miclet, J. Boisbouvier and A. Bax, *J. Biomol. NMR*, 2005, **31**, 201–216.
103. C. P. Jaroniec, J. Boisbouvier, I. Tworowska, E. P. Nikonowicz and A. Bax, *J. Biomol. NMR*, 2005, **31**, 231–241.
104. P. Vallurupalli and P. B. Moore, *J. Biomol. NMR*, 2002, **24**, 63–66.
105. Z. Wu, N. Tjandra and A. Bax, *J. Biomol. NMR*, 2001, **19**, 367–370.
106. T. Carlomagno, M. Hennig and J. R. Williamson, *J. Biomol. NMR*, 2002, **22**, 65–81.
107. J. Boisbouvier, F. Delaglio and A. Bax, *Proc. Natl. Acad. Sci. U. S. A.*, 2003, **100**, 11333–11338.
108. E. Miclet, E. O'Neil-Cabello, E. P. Nikonowicz, D. Live and A. Bax, *J. Am. Chem. Soc.*, 2003, **125**, 15740–15741.
109. M. P. Latham and A. Pardi, *J. Biomol. NMR*, 2009, **43**, 121–129.
110. M. R. Hansen, M. Rance and A. Pardi, *J. Am. Chem. Soc.*, 1998, **120**, 11210–11211.
111. L. Kay, P. Keifer and T. Saarinen, *J. Am. Chem. Soc.*, 1992, **114**, 10663–10665.
112. A. G. Tzakos, L. E. Easton and P. J. Lukavsky, *J. Am. Chem. Soc.*, 2006, **128**, 13344–13345.
113. B. Luy and J. P. Marino, *J. Biomol. NMR*, 2001, **20**, 39–47.

114. A. L. Hansen and H. M. Al-Hashimi, *J. Magn. Reson.*, 2006, **179**, 299–307.
115. A. Grishaev, L. Yao, J. Ying, A. Pardi and A. Bax, *J. Am. Chem. Soc.*, 2009, **131**, 9490–9491.
116. Z. Wu, N. Tjandra and A. Bax, *J. Am. Chem. Soc.*, 2001, **123**, 3617–3618.
117. Z. Wu, F. Delaglio, N. Tjandra, V. B. Zhurkin and A. Bax, *J. Biomol. NMR*, 2003, **26**, 297–315.
118. D. L. Bryce, A. Grishaev and A. Bax, *J. Am. Chem. Soc.*, 2005, **127**, 7387–7396.
119. R. S. Lipsitz and N. Tjandra, *J. Magn. Reson.*, 2003, **164**, 171–176.
120. F. Hallwass, M. Schmidt, H. Sun, A. Mazur, G. Kummerlowe, B. Luy, A. Navarro-Vazquez, C. Griesinger and U. M. Reinscheid, *Angew. Chem., Int. Ed.*, 2011, **50**, 9487–9490.
121. Q. Zhang and H. M. Al-Hashimi, *Nat. Methods*, 2008, **5**, 243–245.
122. C. Musselman, S. W. Pitt, K. Gulati, L. L. Foster, I. Andricioaei and H. M. Al-Hashimi, *J. Biomol. NMR*, 2006, **36**, 235–249.
123. M. H. Bailor, C. Musselman, A. L. Hansen, K. Gulati, D. J. Patel and H. M. Al-Hashimi, *Nat. Protoc.*, 2007, **2**, 1536–1546.
124. S. A. Showalter and K. B. Hall, *Methods Enzymol*, 2005, **394**, 465–480.
125. M. M. Getz, A. J. Andrews, C. A. Fierke and H. M. Al-Hashimi, *RNA*, 2007, **13**, 251–266.
126. X. Sun, Q. Zhang and H. M. Al-Hashimi, *Nucleic Acids Res.*, 2007, **35**, 1698–1713.
127. Q. Zhang, X. Sun, E. D. Watt and H. M. Al-Hashimi, *Science*, 2006, **311**, 653–656.
128. Q. Zhang and H. M. Al-Hashimi, *RNA*, 2009, **15**, 1941–1948.
129. C. Musselman, Q. Zhang, H. Al-Hashimi and I. Andricioaei, *J. Phys. Chem. B*, 2010, **114**, 929–939.
130. J. L. Weaver and J. H. Prestegard, *Biochemistry*, 1998, **37**, 116–128.
131. M. W. Fischer, J. A. Losonczi, J. L. Weaver and J. H. Prestegard, *Biochemistry*, 1999, **38**, 9013–9022.
132. A. J. Dingley and S. Grzesiek, *J. Am. Chem. Soc.*, 1998, **120**, 8293–8297.
133. M. Zweckstetter and A. Bax, *J. Biomol. NMR*, 2002, **23**, 127–137.
134. H. M. Al-Hashimi, A. Gorin, A. Majumdar, Y. Gosser and D. J. Patel, *J. Mol. Biol.*, 2002, **318**, 637–649.
135. H. M. Al-Hashimi and D. J. Patel, *J. Biomol. NMR*, 2002c**22**, 1–8.
136. K. B. Briggman and J. R. Tolman, *J. Am. Chem. Soc.*, 2003, **125**, 10164–10165.
137. H. M. Al-Hashimi, Y. Gosser, A. Gorin, W. Hu, A. Majumdar and D. J. Patel, *J. Mol. Biol.*, 2002b**315**, 95–102.
138. G. M. Clore and C. D. Schwieters, *Biochemistry*, 2004, **43**, 10678–10691.
139. C. D. Schwieters and G. M. Clore, *Biochemistry*, 2007, **46**, 1152–1166.
140. C. K. Fisher and H. M. Al-Hashimi, *J. Phys. Chem. B*, 2009, **113**, 6173–6176.

141. Y. Chen, S. L. Campbell and N. V. Dokholyan, *Biophys. J.*, 2007, **93**, 2300–2306.
142. B. Richter, J. Gsponer, P. Varnai, X. Salvatella and M. Vendruscolo, *J. Biomol. NMR*, 2007, **37**, 117–135.
143. M. Vendruscolo, *Curr. Opin. Struct. Biol.*, 2007, **17**, 15–20.
144. M. R. Jensen, P. R. Markwick, S. Meier, C. Griesinger, M. Zweckstetter, S. Grzesiek, P. Bernado and M. Blackledge, *Structure*, 2009, **17**, 1169–1185.
145. G. M. Clore and C. D. Schwieters, *J. Am. Chem. Soc.*, 2004, **126**, 2923–2938.
146. G. Nodet, L. Salmon, V. Ozenne, S. Meier, M. R. Jensen and M. Blackledge, *J. Am. Chem. Soc.*, 2009, **131**, 17908–17918.
147. N. Sibille, A. Pardi, J. P. Simorre and M. Blackledge, *J. Am. Chem. Soc.*, 2001, **123**, 12135–12146.
148. O. M. Ottink, S. M. Rampersad, M. Tessari, G. J. Zaman, H. A. Heus and S. S. Wijmenga, *RNA*, 2007, **13**, 2202–2212.
149. H. M. Al-Hashimi, Y. Gosser, A. Gorin, W. Hu, A. Majumdar and D. J. Patel, *J. Mol. Biol.*, 2002, **315**, 95–102.
150. E. A. Dethoff, A. L. Hansen, C. Musselman, E. D. Watt, I. Andricioaei and H. M. Al-Hashimi, *Biophys. J.*, 2008, **95**, 3906–3915.
151. M. H. Bailor, X. Sun and H. M. Al-Hashimi, *Science*, 2010, **327**, 202–206.
152. A. M. Mustoe, M. H. Bailor, R. M. Teixeira, C. L. Brooks III and H. M. Al-Hashimi, *Nucleic Acids Res.*, 2011. 4
153. M. H. Bailor, A. M. Mustoe, C. L. Brooks III and H. M. Al-Hashimi, *Curr. Opin. Struct. Biol.*, 2011, **21**, 296–305.
154. S. W. Pitt, Q. Zhang, D. J. Patel and H. M. Al-Hashimi, *Angew. Chem., Int. Ed.*, 2005, **44**, 3412–3415.
155. A. C. Stelzer, J. D. Kratz, Q. Zhang and H. M. Al-Hashimi, *Angew. Chem., Int. Ed.*, 2010, **49**, 5731–5733.
156. A. Casiano-Negroni, X. Sun and H. M. Al-Hashimi, *Biochemistry*, 2007, in press.
157. Q. Zhang, N. K. Kim, R. D. Peterson, Z. Wang and J. Feigon, *Proc. Natl. Acad. Sci. U. S. A.*, 2010, **107**, 18761–18768.
158. T. I. Igumenova, U. Brath, M. Akke and A. G. Palmer III, *J. Am. Chem. Soc.*, 2007, **129**, 13396–13397.
159. A. J. Baldwin, D. F. Hansen, P. Vallurupalli and L. E. Kay, *J. Am. Chem. Soc.*, 2009, **131**, 11939–11948.
160. H. van Ingen, D. M. Korzhnev and L. E. Kay, *J. Phys. Chem. B*, 2009, **113**, 9968–9977.
161. A. C. Stelzer, A. T. Frank, M. H. Bailor, I. Andricioaei and H. M. Al-Hashimi, *Methods*, 2009, **49**, 167–173.